IOP Publishing and International Atomic Energy Agency Nuclear Fusion
Nucl. Fusion **49** (2009) 055001 (9pp) doi:10.1088/0029-5515/49/5/055001

Study of turbulent fluctuations driven by the electron temperature gradient in the National Spherical Torus Experiment

E. Mazzucato[1,4], R.E. Bell[1], S. Ethier[1], J.C. Hosea[1], S.M. Kaye[1], B.P. LeBlanc[1], W.W. Lee[1], P.M. Ryan[2], D.R. Smith[1], W.X. Wang[1], J.R. Wilson[1] and H. Yuh[3]

[1] Princeton Plasma Physics Laboratory, Princeton University, Princeton, NJ 08543, USA
[2] Oak Ridge National Laboratory, Oak Ridge, TN 37831, USA
[3] Nova Photonics Inc., Princeton, NJ 08540, USA

E-mail: mazzucato@pppl.gov

Received 29 December 2008, accepted for publication 17 March 2009
Published 9 April 2009
Online at stacks.iop.org/NF/49/055001

Abstract
Various theories and numerical simulations support the conjecture that the ubiquitous problem of anomalous electron transport in tokamaks may arise from a short-scale turbulence driven by the electron temperature gradient. To check whether this turbulence is present in plasmas of the National Spherical Torus Experiment, measurements of turbulent fluctuations were performed with coherent scattering of electromagnetic waves. Results from plasmas heated by high harmonic fast waves show the existence of density fluctuations in the range of wave numbers $k_\perp \rho_e = 0.1$–0.4, corresponding to a turbulence scale length of the order of the collisionless skin depth. Experimental observations and agreement with numerical results from the linear gyro-kinetic GS2 code indicate that the observed turbulence is driven by the electron temperature gradient. These turbulent fluctuations were not observed at the location of an internal transport barrier driven by a negative magnetic shear.

PACS numbers: 52.55.Fa, 52.35.Qz, 52.35.Ra

1. Introduction

Understanding the mechanism of plasma transport in tokamaks is one of the great challenges of fusion research. Indeed, since most explanations of this phenomenon are based on some type of turbulence [1–3], understanding plasma transport depends upon understanding turbulence. Unfortunately, since this is a tremendously difficult problem, the cause of anomalous energy losses in tokamaks is still an outstanding issue.

Particularly difficult to explain is the transport of electron energy. This is the most worrisome since in a tokamak reactor a large fraction of the energy of charged fusion products—necessary to sustain the nuclear fusion reactions—would be released directly to the electrons. Various theories and numerical simulations [4–10] support the conjecture that anomalous electron transport may arise from a turbulence driven by the electron temperature gradient (ETG) instability. Until recently, however, very little was known experimentally on the existence of a short-scale turbulence driven by the ETG in tokamaks. Fortunately, recent experiments are beginning to fill this gap [11–17].

To investigate this type of turbulence, a series of experiments have been performed in plasmas of the National Spherical Torus Experiment (NSTX). These plasmas are uniquely suited for the study of the physics of electron transport since, while the confinement of ions in NSTX is very often at or near neoclassical levels, that of electrons is anomalous in all operational regimes [18]. Preliminary results have been presented in [16]. Here, we give a more detailed description of these measurements.

2. Coherent scattering of electromagnetic waves

Short-scale density fluctuations were measured with coherent scattering of electromagnetic waves, a powerful technique that was used extensively in early studies of plasma turbulence, including the first detection of short-scale turbulent fluctuations in tokamaks [19]. The process can be characterized by an effective differential cross section per unit

[4] Author to whom any correspondence should be addressed.

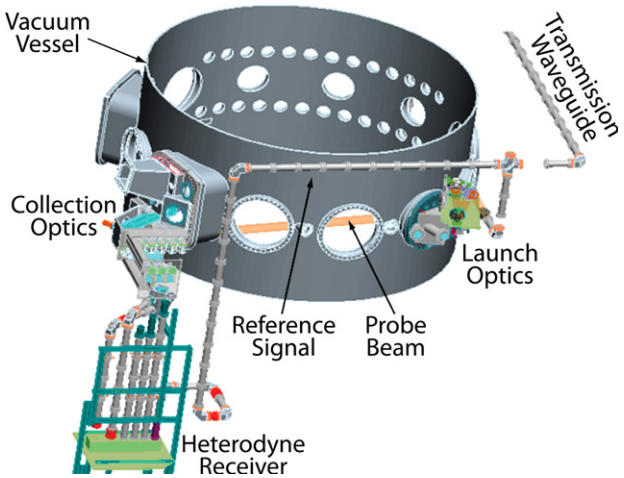

Figure 1. Arrangement of main components of the NSTX scattering system.

volume

$$\sigma = r_0^2 S(\boldsymbol{k}, \omega), \tag{1}$$

where $r_0 = e^2/mc^2$ is the classical radius of electrons and $S(\boldsymbol{k}, \omega)$ is the spectral density of fluctuations [20]. The mean square density fluctuation is obtained from

$$\left\langle |\tilde{n}_e|^2 \right\rangle = \frac{1}{(2\pi)^4} \int S(\boldsymbol{k}, \omega)\, \mathrm{d}\boldsymbol{k}\, \mathrm{d}\omega. \tag{2}$$

Frequency (ω) and wave vector ($\boldsymbol{k}$) of measured fluctuations must satisfy the energy and momentum conservation

$$\omega = \omega_s - \omega_i, \qquad \boldsymbol{k} = \boldsymbol{k}_s - \boldsymbol{k}_i, \tag{3}$$

where the superscripts s and i refer to scattered and incident waves, respectively. Since for the topic of this paper $\omega_s \approx \omega_i$ and $k_s \approx k_i$, the scattering angle θ must satisfy the Bragg condition $k = 2k_i \sin(\theta/2)$.

The NSTX scattering system (figure 1) employs a probing wave with a frequency of 280 GHz, together with a five-channel heterodyne receiver capable of providing full information on the frequency spectrum of measured signals [21]. The unique feature of the scattering geometry is the oblique propagation of the probing beam with respect to the magnetic field, with both probe and scattered waves lying nearly on the equatorial midplane (figure 2). Consequently, the wave vectors ($\boldsymbol{k}$) of measured fluctuations are almost perpendicular to the magnetic surfaces, albeit with small components in both diamagnetic and toroidal directions from which one could infer the velocity of propagation in the plasma frame. Note that in figure 2, $\boldsymbol{k}$ is pointing outwards for inboard fluctuations, and inwards for outboard fluctuations. This, together with the near perpendicularity of $\boldsymbol{k}$ to the magnetic field (see below), forces all components of $\boldsymbol{k}$ to have opposite signs in the two scattering configurations [22, 23], as illustrated in figure 3, showing the wave vector components of measured fluctuations from a ray tracing code. Hence, for the same type of plasma turbulence, i.e. having the same direction of propagation in the plasma frame, any frequency Doppler shift of measured signals should have opposite signs in the two scattering configurations.

The instrumental resolution of scattering measurements is limited by the size of the probing and scattered beams, both having a Gaussian profile with a radius (a) of 2.5 cm in the present experiment. If we take the size of the region that the two beams have in common as a measure of spatial resolution (δl), we get $\delta l = 4k_i a/k$, that in our case gives $\delta l = 60$ cm for $k = 10\,\mathrm{cm}^{-1}$. From this, we might conclude that it is difficult to perform localized measurements of plasma turbulence with coherent scattering of electromagnetic waves. Fortunately, this estimate is valid only for an isotropic turbulence, which is not the case of tokamak plasmas where short-scale fluctuations satisfy the relation $\boldsymbol{k}\cdot\boldsymbol{B}/B \approx 1/qR$ [1, 2] (with $\boldsymbol{B}$ the magnetic field, q the magnetic safety factor and R the plasma major radius). For all practical purposes, then, we can assume

$$\boldsymbol{k}\cdot\boldsymbol{B} = 0, \tag{4}$$

which, because of the large curvature of magnetic field lines, makes the instrumental selectivity function, i.e. the collection efficiency of scattered waves, strongly localized [22, 23]. This can be seen by considering scattered waves originating from two points of the probing beam with wave vectors $\boldsymbol{k}_s^1$ and $\boldsymbol{k}_s^2$, respectively. From figure 4, we get

$$\frac{\boldsymbol{k}_s^1\cdot\boldsymbol{k}_s^2}{k_i^2} \equiv \cos\alpha = \cos\theta_1\cos\theta_2 + \sin\theta_1\sin\theta_2 \times (\cos\varphi_1\cos\varphi_2 + \sin\varphi_1\sin\varphi_2)\,, \tag{5}$$

giving

$$\cos\alpha = \cos(\theta_2 - \theta_1) - 2\sin\theta_1\sin\theta_2\sin^2(\delta\varphi/2), \tag{6}$$

where $\delta\varphi = \varphi_2 - \varphi_1$. Since in this experiment both scattering angles θ_1 and θ_2 are small, we may write

$$\alpha^2 \approx (\theta_2 - \theta_1)^2 + 4\theta_2\theta_1\sin^2(\delta\varphi/2). \tag{7}$$

Then, if the receiving antenna is positioned for collecting with maximum efficiency the scattered waves from the first point, those from the second will be collected with the relative efficiency $\exp(-\alpha^2/\alpha_0^2)$, where $\alpha_0 = 2/k_i a$ [22, 23]. From this and equation (7), we obtain the instrumental selectivity function

$$F = \exp\left[-\left((k'-k)^2 + 4k'k\sin^2(\delta\varphi/2)\right)/\Delta^2\right], \tag{8}$$

where $\Delta = 2/a$, $k \approx k_i\theta_1$ is the tuning wave number of the receiving antenna and $k' \approx k_i\theta_2$ is the wave number of detected fluctuations. The contour plot of F as a function of position s along the probing beam (with $s = 0$ at the plasma boundary) and the wave number mismatch ($\Delta k = k' - k$) is shown in figure 5, where the value of $\delta\varphi$ is from a ray tracing code using the equilibrium reconstruction code EFIT [24] together with equations (3) and (4). This shows that indeed the length of the scattering region is substantially smaller than the above estimate for the case of isotropic turbulence. In addition, because of the novel scattering geometry, the radial footprint of the scattering region is very close to the diameter of the probing beam ($2a$), so that the radial resolution of our fluctuation measurements is ± 2.5 cm together with a wave number resolution of $\pm 1\,\mathrm{cm}^{-1}$.

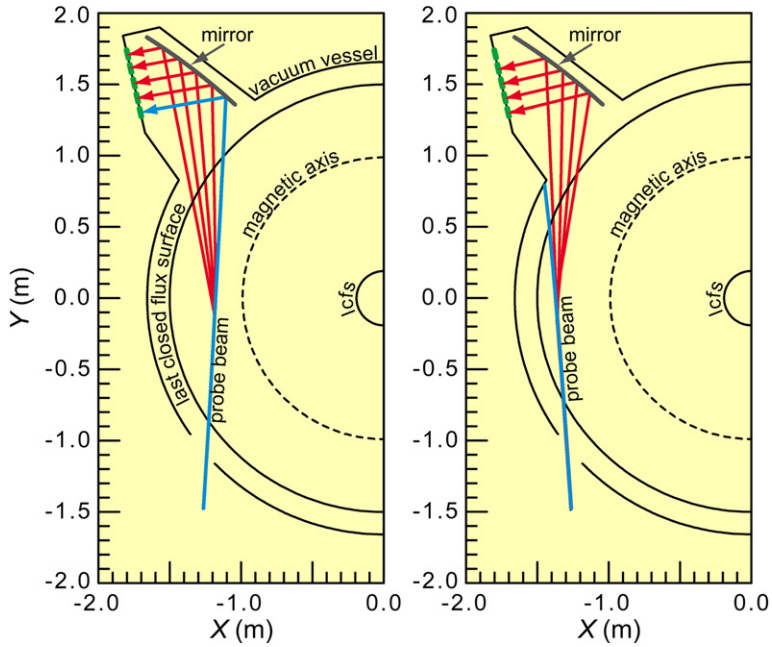

Figure 2. Probe beam (blue) and scattered waves (red) for detection of inboard (left) and outboard (right) fluctuations. Steerable optics can position the scattering region from the magnetic axis to the plasma edge.

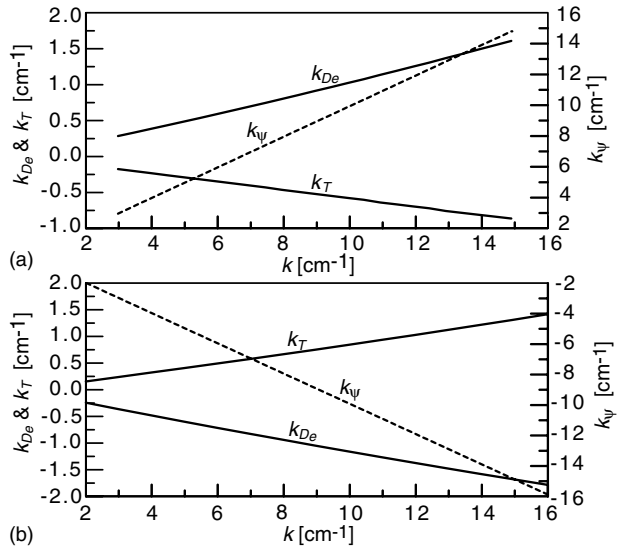

Figure 3. Wave vector components of measured fluctutions as a function of $k = |\boldsymbol{k}|$: k_ψ is along the outward normal to the magnetic surface; k_{De} is along the electron diamagnetic velocity; k_T is along the toroidal current ((*a*) inboard fluctuations and (*b*) outboard fluctuations).

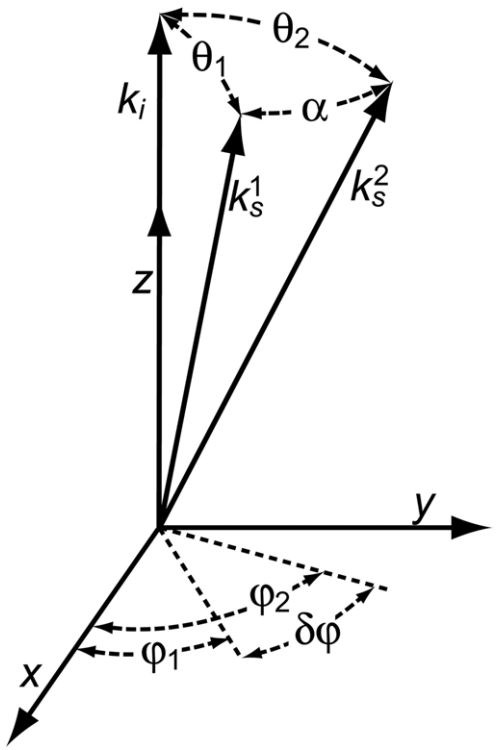

Figure 4. Orthogonal coordinates (x, y, z) with the z-axis along the wave vector of probing beam.

3. Results

The experimental results presented in this paper were obtained in plasmas with high harmonic fast wave (HHFW) heating [25]. Use of this radio frequency (RF) technique—where a wave with the frequency (30 MHz) of an ion cyclotron harmonic (∼10th) is absorbed by the electrons—was motivated by its ability to produce electron temperature (T_{e}) profiles with large central values and steep gradients. An example is illustrated in figures 6 and 7, showing the case of a helium discharge with a minor radius of 0.65 m, a major radius of 0.85 m, an elongation of 2, a toroidal magnetic field of 0.55 T, a plasma current of 700 kA and an RF-heating power of 1.2 MW. Use of the maximum available magnetic field and of relatively low plasma current was motivated by the need to minimize the spurious effects of MHD turbulence. In addition, because of the low plasma density, i.e. a weak electron–ion coupling, the

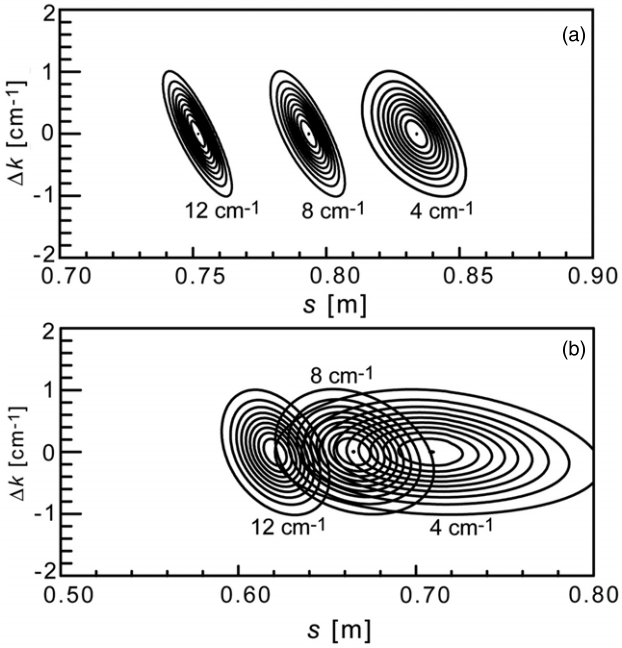

Figure 5. Contour plot of F (ten levels equally spaced from 0.1 to 1, with maximum at $\Delta k = 0$) as a function of position s along the probe beam (with $s = 0$ at plasma boundary) and $\Delta k = k' - k$ ((*a*) inboard fluctuations and (*b*) outboard fluctuations). Labels are values of k.

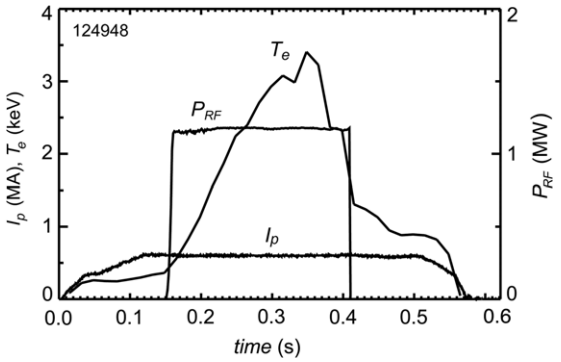

Figure 6. Time evolution of plasma current (I_p), RF power (P_{RF}) and peak electron temperature (T_e).

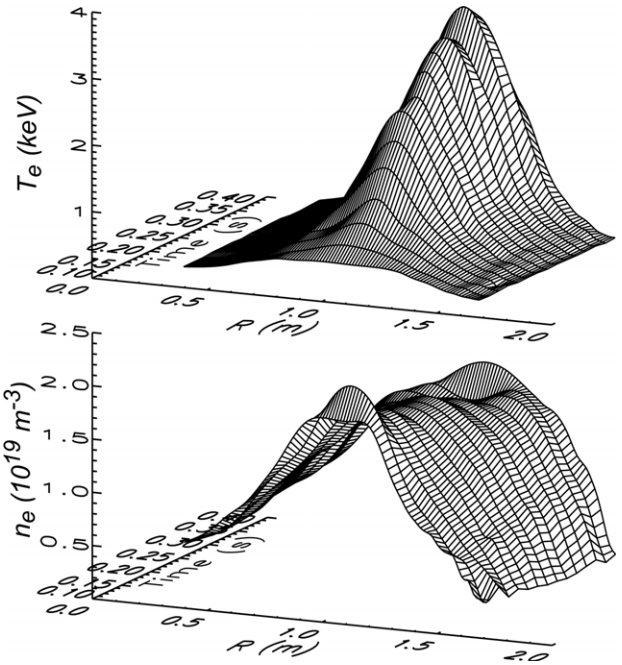

Figure 7. Radial profiles of electron temperature T_e (top) and density n_e (bottom) in plasmas with 1.2 MW of HHFW heating.

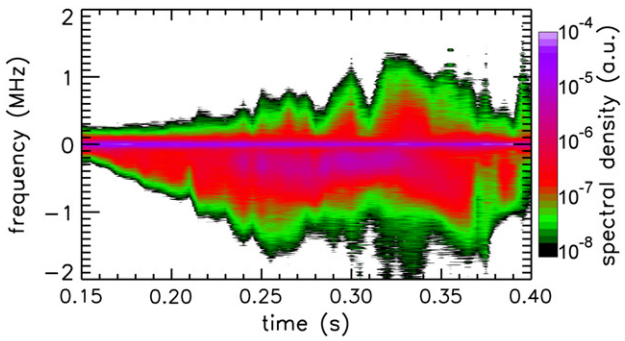

Figure 8. Logarithmic contour plot of the spectral density of fluctuations with $k_\perp \rho_e = 0.2$–0.4 at $r/a = 0.3$. Negative frequencies correspond to wave propagation in the electron diamagnetic direction.

ion temperature (T_i) remained nearly constant (with central values of 0.8–1.0 keV).

Figure 8 shows the time evolution of the spectral density of fluctuations with $k_\perp = 14\,\mathrm{cm}^{-1}$ at $r/a = 0.3$ ($R = 1.2$ m), corresponding to the range of $k_\perp \rho_e = 0.2$–0.4 (with ρ_e the electron gyro-radius), $k_\perp \rho_s = 8.5$–17 (with ρ_s the ion gyro-radius at the electron temperature) and $k_\perp \rho_i = 8$–10 (with ρ_i the ion gyro-radius). The latter implies that the source of observed fluctuations is not the ion temperature gradient (ITG) mode, which is instead characterized by $k_\perp \rho_i < 1$ [1–3]. This mode is also excluded by the frequency asymmetry of measured spectra, as shown in figure 8, indicating that fluctuations propagate in the electron diamagnetic direction. Finally, the large values of $k_\perp \rho_s$ seem to exclude the trapped electron mode (TEM) as well.

It is interesting to note that for the plasma density in figure 7, $k_\perp \delta_{sk} \sim 2$, where δ_{sk} is he collisionless skin depth ($c/\omega_{pe} = \rho_e/\beta_e^{1/2}$), with ω_{pe} the plasma frequency and β_e the electron beta. This is not surprising since for sufficiently large values of β_e, such as those in the present experiment (3–6%), the characteristic turbulence scale length is expected to be of the order of the collisionless skin depth [4, 26].

These turbulent fluctuations appear to be related to the electron temperature gradient, as illustrated in figure 9 where the frequency integrated value of the spectral density (S_{tot}) is compared with the electron temperature scale length (defined as $L_{Te} = (\mathrm{d} \ln T_e/\mathrm{d}r)^{-1}$) at the location of measurement. Note that plasma fluctuations begin to rise at the beginning of the RF pulse, when the value of L_{Te} begins to drop, and decrease towards the end of the pulse when the opposite occurs.

The same phenomenon is illustrated in figure 10, showing the electron temperature profile and the spectrum of measured fluctuations at two different times, the first when the amplitude of fluctuations is maximum (0.3 s), the second after the RF pulse (0.43 s) when the profile of T_e has collapsed and flattened

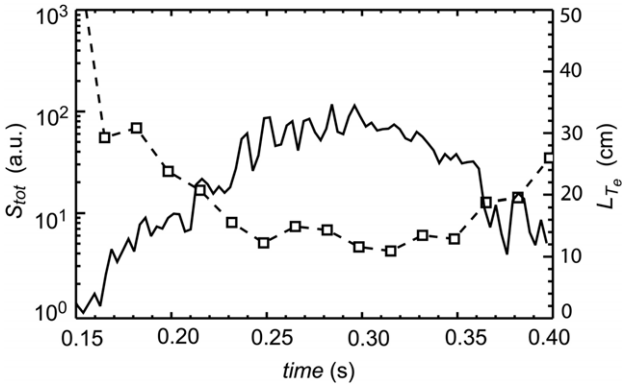

Figure 9. Frequency integrated spectral density $S_{\rm tot}$ (solid line) and radial scale $L_{\rm Te}$ (dash line) for the case of figure 8.

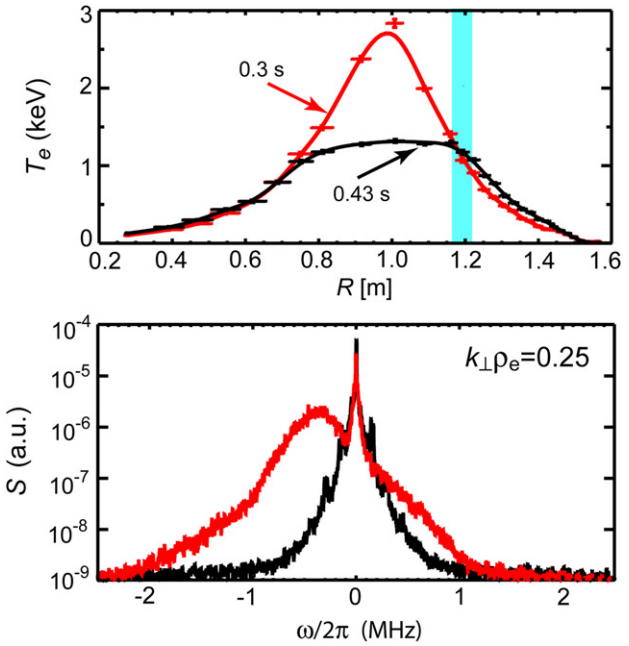

Figure 10. Temperature profiles (top) and spectral density of fluctuations (bottom) at 0.3 (red) and 0.43 s (black). The blue stripe indicates the location of measurement where $L_{\rm Te}$ is 15 cm and 50 cm, respectively. Negative frequencies (bottom) correspond to wave propagation in the electron diamagnetic direction.

over a wide central region. At the location of measurement (blue stripe in figure 10), both ion and electron temperatures and plasma densities are the same in both cases, while the values of $L_{\rm Te}$ differ by a factor of three (15 versus 50 cm). Correspondingly, while both spectra contain a central narrow symmetric feature—caused by spurious stray radiation—that at 0.3 s displays a strong Doppler shifted component, which is that of scattering signals from large plasma fluctuations. These results clearly demonstrate the dependence of measured turbulence on the radial scale of $T_{\rm e}$.

Short-scale turbulent fluctuations were also detected on the outer region of the plasma column ($r/a = 0.6$), as illustrated in figure 11 showing the spectral density of fluctuations with wave numbers in the range $k_\perp\rho_{\rm e} = 0.1$–$0.2$ and $k_\perp\rho_{\rm i} \approx k_\perp\rho_{\rm s} = 4$–$8$. Again, the scale length is of the order of the collisionless skin depth ($k_\perp\delta_{\rm sk} = 1$–$2$). As in the case of core fluctuations, wave numbers are outside the range of both

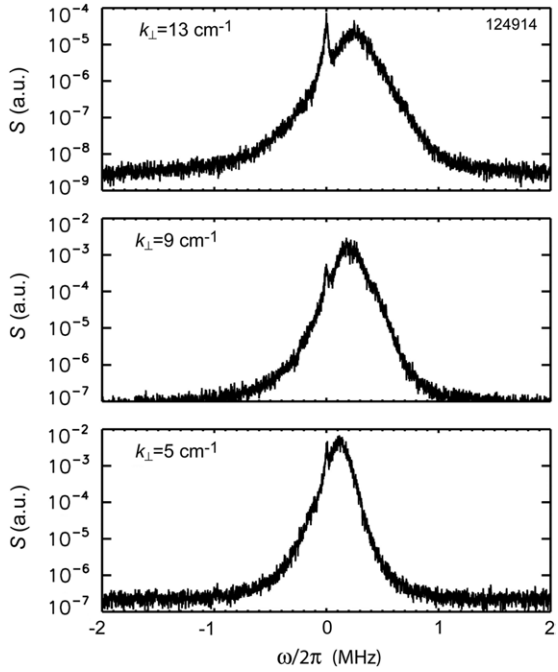

Figure 11. Spectral density of fluctuations in the range of wave numbers $k_\perp\rho_{\rm e} = 0.1$–$0.2$ at $r/a = 0.6$. Positive frequencies correspond to wave propagation in the electron diamagnetic direction.

ITG and TEM modes, and wave propagation is in the electron diamagnetic direction (corresponding to positive frequencies for the scattering geometry used for these measurements).

Proof of a propagation of observed fluctuations along the electron diamagnetic direction is of crucial importance since it rules out the ITG instability as the source of turbulence. So far in the present paper, the phase propagation of fluctuations was inferred from the sign of measured frequencies when the Doppler shift from a toroidal plasma rotation was negligible, i.e. from the sign of $(\omega_{\rm s} - \omega_{\rm i})$ together with the wave vector component of measured fluctuations in the diamagnetic direction. Indeed, the Doppler shift from a plasma rotation could provide further information on the direction of wave propagation. This can be understood using the orthogonal system of coordinates (θ, φ, ψ) in figure 12, where the unit vector $\boldsymbol{e}_\psi$ is in the outward normal direction to the magnetic surface (i.e. $\nabla p \cdot \boldsymbol{e}_\psi < 0$), and $\boldsymbol{e}_\varphi$ is parallel to the toroidal plasma current (i.e. $B_\theta > 0$). For short, let us refer to fluctuations that in the plasma frame propagate along the electron diamagnetic velocity ($\boldsymbol{v}_{\rm De} = \nabla p_{\rm e} \times \boldsymbol{B}/en_{\rm e}B^2$) as electron waves, and those propagating along the ion diamagnetic velocity ($\boldsymbol{v}_{\rm Di} = -\nabla p_{\rm i} \times \boldsymbol{B}/en_{\rm i}B^2$) as ion waves. From equation (4)—implying that the projection on the magnetic surface of the wave vector of fluctuations is parallel to the plasma diamagnetic velocity—and from

$$\boldsymbol{v}_{\rm De} \cdot \boldsymbol{e}_\varphi = -\frac{|\nabla p_{\rm e}| B_\theta}{en_{\rm e}B^2} < 0 \qquad (9)$$

we conclude that for electron waves, a plasma co-rotation (i.e. in the plasma current direction) should induce a Doppler shift of measured spectra with the opposite sign of the intrinsic frequency of fluctuations i.e. when measured in the absence

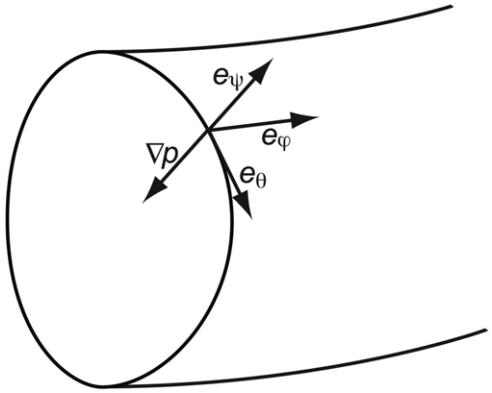

Figure 12. Orthogonal coordinate system (θ, φ, ψ) with $\boldsymbol{e}_\psi$ long the outward normal to the magnetic surface and $\boldsymbol{e}_\varphi$ parallel to the toroidal plasma current.

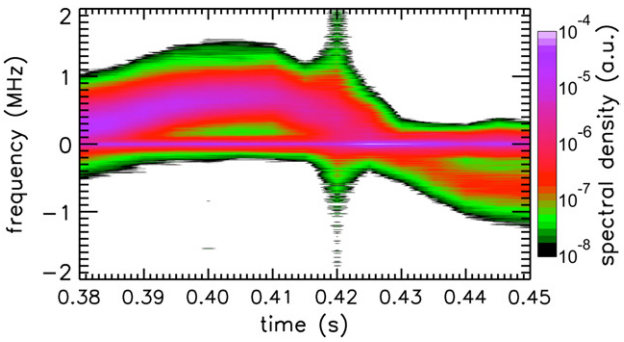

Figure 13. Time evolution of the spectrum of fluctuations with $k_\perp = 13\,\mathrm{cm}^{-1}$ for the plasma rotation of figure 14 (burst at 0.42 s was caused by the abrupt termination of the RF pulse by the onset of an MHD instability).

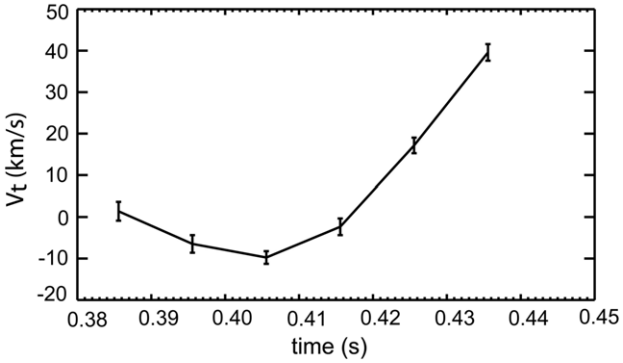

Figure 14. Time evolution of toroidal plasma velocity v_t (positive when along the plasma current).

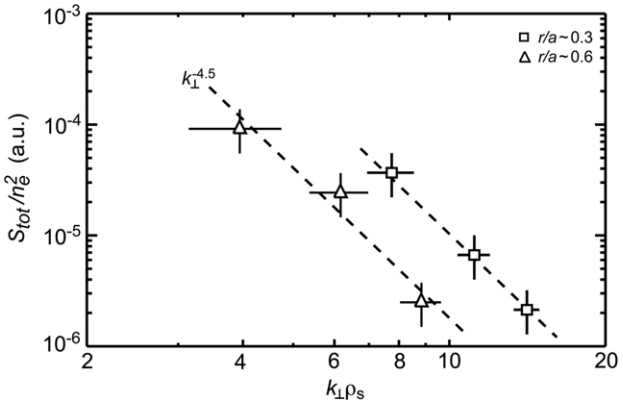

Figure 15. Power spectrum of fluctuations (normalized to the square of local density) as a function of $k_\perp\rho_s$ for both inboard (squares) and outboard (triangles) measurements.

of plasma rotation. (In other words, if the latter is negative, the measured frequency should increase; if positive, the measured frequency should decrease.) Then, from

$$\boldsymbol{v}_{\mathrm{Di}} \cdot \boldsymbol{e}_\varphi = \frac{|\nabla p_\mathrm{i}| B_\theta}{e n_\mathrm{e} B^2} > 0, \tag{10}$$

we get that all of the above should be reversed for the case of ion waves. Finally, it is obvious that the Doppler shift from a plasma counter-rotation is just the opposite of that induced by a plasma co-rotation.

In the case of heterodyne detection, such as that used in the present experiment [21], the sign of measured frequencies is a byproduct of the detection system itself, since it depends on whether the frequency of the first local oscillator is larger or smaller than the frequency of the probing beam. However, what has a physical meaning is the difference between the frequency of the probing beam and that of scattered waves, whose sign is not necessarily that of the frequency of measured signals. It is important to note that from the above explanation of Doppler shifts, the propagation of fluctuations is derived without any knowledge of the heterodyne receiver setting.

Figures 13 and 14, which display the time evolution of the spectrum of fluctuations and of the plasma toroidal velocity v_t (driven in part by the neutral beam used for velocity measurements with the method of charge exchange recombination spectroscopy), demonstrate that the frequency follows the toroidal velocity as just described for the case of electron waves, while it disagrees completely with what to expect for ion waves, since in this case the measured frequency—that in figure 14 is positive when $v_t = 0$—should decrease when $v_t < 0$ and increase when $v_t > 0$. Hence the conclusion that the observed fluctuations propagate in the electron diamagnetic direction.

Finally, the power spectrum of fluctuations (i.e. the value of S_{tot} normalized to n_e^2) is displayed in figure 15 as a function of $k_\perp\rho_\mathrm{s}$ for both inboard (figure 8) and outboard (figure 11) measurements. Surprisingly, the power spectrum follows a similar power law ($\sim k_\perp^{-4.5}$) at both plasma locations in spite of different electron temperatures (1.5 versus 0.5 keV). If the measured fluctuations were isotropic perpendicularly to the magnetic field—impossible to prove with our measurements—the mean square density fluctuation would follow the power law $\langle|\tilde{n}_\mathrm{e}^2|\rangle/n_\mathrm{e}^2 \propto k_\perp^{-3.5}$.

4. Negative magnetic shear

It is known that a negative magnetic shear can induce—under certain conditions—the formation of internal transport barriers (ITB), resulting in drastically reduced outflow of plasma energy. The signature of an electron ITB is a sharp temperature gradient at the barrier location, inside which the profile of T_e is nearly flat. If the turbulent fluctuations described in this paper are responsible—even partially—for the electron anomalous

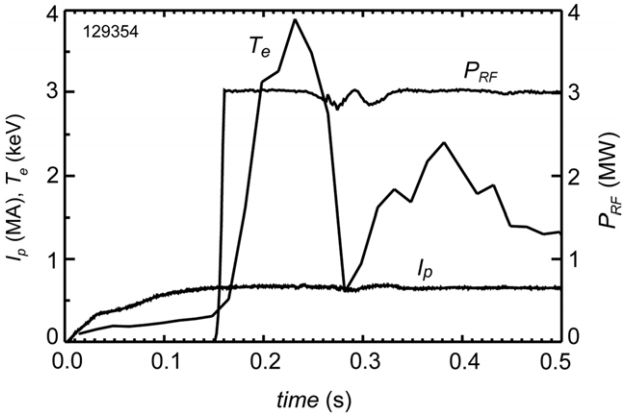

Figure 16. Time evolution of plasma current (I_p), RF power (P_{RF}) and peak electron temperature (T_e) in a plasma with negative magnetic shear.

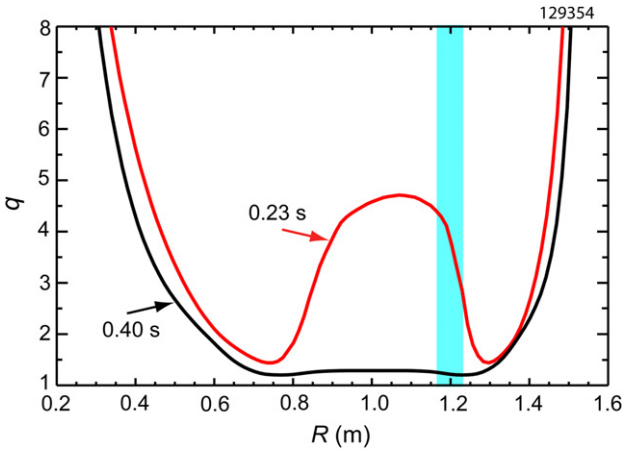

Figure 17. Magnetic safety factor on the equatorial plane at the peak of T_e (red) and after the collapse of negative magnetic shear (black). The blue stripe indicates the location of fluctuation measurements.

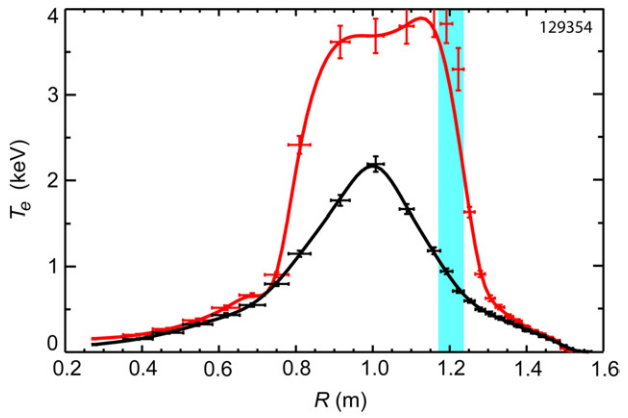

Figure 18. Same as in figure 17 for T_e (red line: $t = 0.23$ s; black line: $t = 0.4$ s).

transport in tokamaks, they should be suppressed at the location of an electron ITB.

A simple procedure for producing NSTX plasmas with negative magnetic shear is launching a high power HHFW pulse during the early phases of a discharge, when the toroidal current is still diffusing from the plasma edge to the centre.

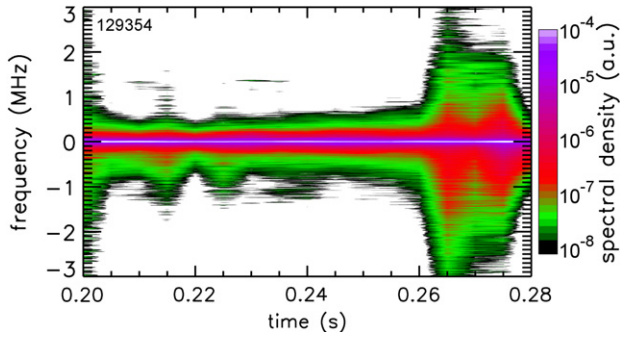

Figure 19. Spectral density of measured fluctuations (same scattering geometry as in the case of figure 8 with $k_\perp = 12\,\mathrm{cm}^{-1}$) during a negative reversed shear. The sudden rise at $t = 0.26$ coincides with the collapse of the ITB.

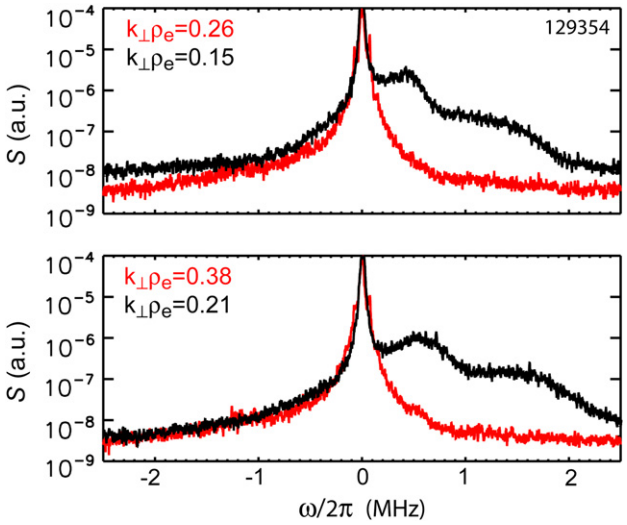

Figure 20. Same as in figure 18 for the spectrum of fluctuations (red: $t = 0.23$ s; black: $t = 0.4$ s).

An example is shown in figure 16, where 3 MW of RF-heating were injected into a deuterium plasma. The resulting strong electron heating together with a low value of Z_{eff} (∼1.4) had the effect of slowing down the diffusion of plasma current and forming a central region with strong negative magnetic shear, which lasted until the onset of an MHD instability caused a fast redistribution of the plasma current and a flattening of its radial profile (figure 17). During the phase of negative shear, the electron temperature developed a steep gradient near the radius of minimum q (figure 18), which indicates the presence of an ITB [27]. Figures 19 and 20 show that fluctuations were suppressed at the transport barrier, a striking similarity to what was found previously in similar TFTR plasmas [28] (albeit for fluctuations driven by the ITG mode) where the suppression of turbulence was explained as the combined effect of the negative magnetic shear and the $E \times B$ velocity shear. However, turbulent fluctuations reappeared (figure 20) as soon as the plasma current diffused to the plasma core, making the q-profile nearly constant over a wide central region (figure 17). Note that in the latter case, the spectrum of measured fluctuations is mostly in the positive frequency side, which in the absence of a toroidal plasma rotation corresponds to wave propagation in

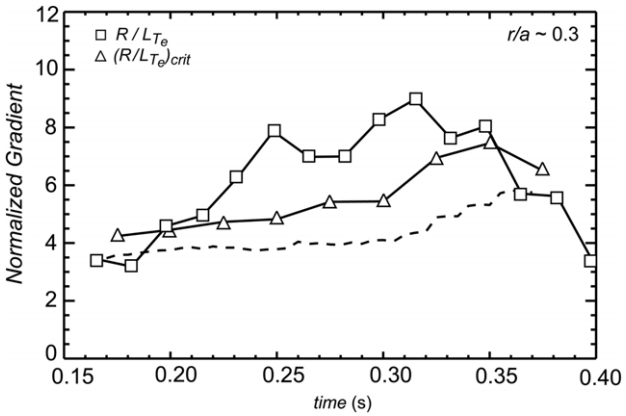

Figure 21. Time evolution of measured gradient R/L_{Te} (squares) and GS2 critical gradient $(R/L_{\mathrm{Te}})_{\mathrm{crit}}$ (triangles) for the onset of the ETG mode in the case of inboard fluctuations (figure 8). The dashed line is the critical gradient from [30].

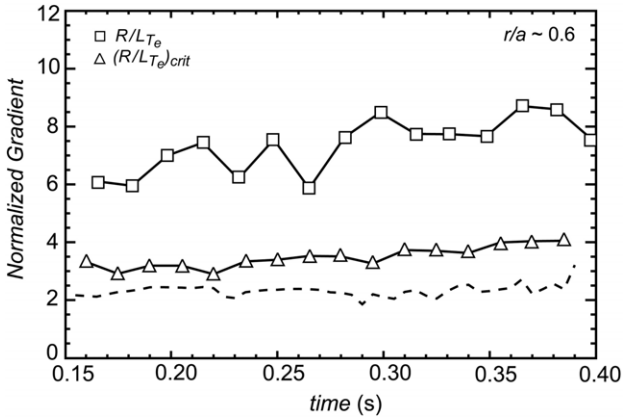

Figure 22. Same as in figure 21 for the case of outboard fluctuations (figure 11).

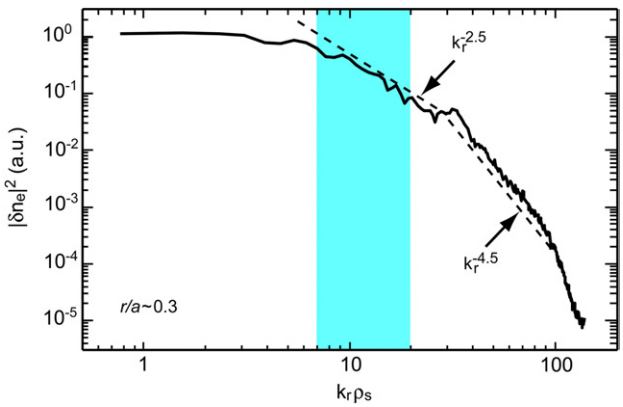

Figure 23. Power spectrum of density fluctuations from the GTS code for a case similar to that with $r/a = 0.3$ in figure 15 (the blue stripe indicates the range of wave numbers of measured fluctuations).

the ion diamagnetic direction. However, this was caused by a large plasma co-rotation—in excess of 80 km s^{-1}—which, as explained in section 3, shifted the spectrum of measured signals from the electron to the ion side.

5. Discussion

In an attempt to determine the source of observed fluctuations, we employed a linear version of the GS2 stability code [29] to obtain the normalized critical gradient $(R/L_{\mathrm{Te}})_{\mathrm{crit}}$ for the onset of the ETG instability. This code solves the gyro-kinetic Vlasov–Maxwell equations, including passing and trapped particles, electromagnetic effects, as well as a Lorentz collision operator. The results are shown in figure 21, where the critical gradient is compared with the measured normalized temperature gradient R/L_{Te} for the case of figure 8. From this, we conclude that the ETG mode is indeed unstable over most of the RF pulse where the critical gradient is smaller than the measured temperature gradient.

Figure 21 also displays an algebraic expression of the normalized critical gradient that was derived in [30] using a best fit of GS2 results for a set of model tokamak configurations. This is given by

$$(R/L_{\mathrm{Te}})_{\mathrm{crit}} = (1 + Z_{\mathrm{eff}}\, T_{\mathrm{e}}/T_{\mathrm{i}})(1.3 + 1.9s/q)(1 - 1.5\varepsilon), \quad (11)$$

where Z_{eff} is the ionic effective charge ($\sim$2.5 in figure 21), $s = r(\mathrm{d}\ln q/\mathrm{d}r)$ is the magnetic shear and $\varepsilon = r/R$ is the inverse aspect ratio. This formula, showing the stabilizing role of Z_{eff}, the temperature ratio $T_{\mathrm{e}}/T_{\mathrm{i}}$ and the magnetic shear, gives values of critical gradient that are not very different from those obtained from the GS2 code using the exact equilibrium configuration of our plasmas.

Similar plots are displayed in figure 22 for the case of outboard fluctuations (figure 11), showing again that fluctuations coincide with a temperature gradient which is larger than the critical gradient. At this plasma location, however, since the HHFW heating did not modify significantly plasma conditions, both the amplitude of measured fluctuations and the ETG critical gradient remained nearly constant in time.

The observed fluctuations were also compared with numerical results of a non-linear simulation of short-scale plasma turbulence using the gyro-kinetic tokamak simulation code (GTS) [31]—a numerical tool capable of providing a global picture of electrostatic turbulence in realistic tokamak configurations. Because of the extremely high resolution required for electron-scale fluctuations, ions were treated adiabatically, i.e. neglecting the coupling to ion-scale fluctuations. This is not a serious problem in NSTX plasmas, where a large $E \times B$ velocity shear suppresses turbulent fluctuations with low wave numbers [18]. More serious is instead the inability of GTS to deal with electromagnetic effects, an extremely difficult problem—if not impossible—for present non-linear gyro-kinetic simulations of plasma turbulence.

Figure 23 shows the calculated power spectrum of density fluctuations as a function of $k_r\rho_{\mathrm{s}}$ for $r/a = 0.3$. It confirms that in the range of measured wave numbers, the spectrum follows a power law, albeit with a different exponential power of -2.5. A nonlinearly generated zonal flow was also observed in the simulation during the development of turbulence. However, the zonal flow is significantly weaker than what is found for ITG turbulence, indicating that radial elongated streamers can survive making fluctuations anisotropic perpendicularly to the magnetic field (figure 24). The length of these streamers ($\sim 150\rho_{\mathrm{e}}$) is outside the range of wavelengths of measured

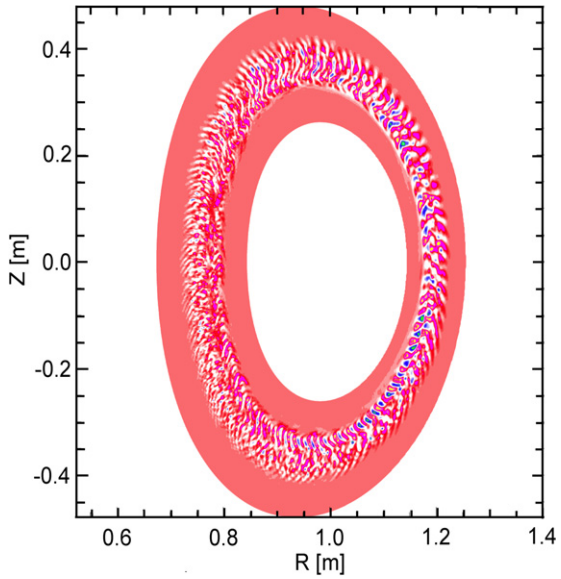

Figure 24. Contour plot of electric potential from the GTS code showing radial streamers. The total width of the plasma annulus is approximately $400\rho_e$.

fluctuations (figure 15). However, we must stress that the GTS simulation finds the presence of fluctuations only on a narrow plasma annulus with a radial width that—surprisingly—is identical to the elongation of streamers. This disagrees with the results of our measurements, indicating instead the existence of fluctuations over a much wider region ($r/a = 0.3$–0.6).

6. Conclusion

In conclusion, turbulent fluctuations have been observed in NSTX plasmas in the range of wave numbers $k_\perp \rho_e = 0.1$–0.4, corresponding to a radial scale of the order of the collisionless skin depth. Large values of $k_\perp \rho_i$, a strong correlation with the scale of T_e and phase propagation in the electron diamagnetic direction exclude the ITG mode as the source of turbulence. Similarly, the large values of $k_\perp \rho_s$ seem to exclude the TEM mode (even though our experiment does not eliminate completely the possibility that measured fluctuations are caused by the non-linear cascade of a long-wavelength TEM turbulence to short-wavelengths). Finally, experimental observations and agreement with numerical results from the linear gyro-kinetic GS2 code support the conjecture that the observed turbulence is driven by the ETG.

These fluctuations were not observed at the location of an ITB driven by a strong negative magnetic shear. Even though this could be used as evidence of the role played on plasma transport by the fluctuations described in this paper, additional experiments together with non-linear numerical simulations of plasma turbulence are needed before reaching any definite conclusion.

Acknowledgments

This work was supported by US Department of Energy Contract No DE-AC02-76CH03073. The authors would like to thank the entire NSTX operations, physics and engineering teams for their contributions to this effort.

References

[1] Coppi B. and Rewoldt G. 1976 *Advances in Plasma Physics* vol 6 ed A Simon and W B Thompson (New York: Wiley) p 421
[2] Horton W. 1999 *Rev. Mod. Phys.* **71** 735
[3] Connor J.W. and Wilson H.R. 1994 *Plasma Phys. Control. Fusion* **36** 719
[4] Horton W., Zhu P., Hoang G.T., Aniel T. and Garbet X. 2000 *Phys. Plasmas* **7** 1494
[5] Dorland W., Jenko F., Kotschereuther M. and Rotgers B.N. 2000 *Phys. Rev. Lett.* **85** 5579
[6] Jenko F. and Dorland W. 2002 *Phys. Rev. Lett.* **89** 225001
[7] Nevins W.M. *et al* 2006 *Phys. Plasmas* **13** 122306
[8] Dimits A.M. *et al* 2007 *Nucl. Fusion* **47** 817
[9] Waltz R.E., Candy J. and Fahey M. 2007 *Phys. Plasma* **14** 0561116
[10] Horton W. *et al* 2004 *Phys. Plasmas* **11** 2600
[11] Gusakov E.Z. *et al* 2006 *Plasma Phys. Control. Fusion* **48** B443
[12] Gusakov E.Z. *et al* 2006 *Plasma Phys. Control. Fusion* **48** A371
[13] Gurchenko A.D. *et al* 2007 *Nucl. Fusion* **47** 245
[14] Rhodes T.L. *et al* 2007 *Nucl. Fusion* **47** 936
[15] Rhodes T.L. *et al* 2007 *Plasma Phys. Control. Fusion* **49** B183
[16] Mazzucato E. *et al* 2008 *Phys. Rev. Lett.* **101** 075001
[17] Gusakov E.Z. *et al* 2008 *Proc. 22nd Int. Conf. on Fusion Energy (Geneva, Switzerland, 2008)* (Vienna: IAEA) CD-ROM file EX/10-2Rb and http://www-naweb.iaea.org/napc/physics/FEC/FEC2008/html/index.htm
[18] Kaye S.M. *et al* 2007 *Phys. Rev. Lett.* **98** 175002
[19] Mazzucato E. 1976 *Phys. Rev. Lett.* **36** 792
[20] Rosenbluth M.N. and Rostoker N. 1962 *Phys. Fluids* **5** 776
[21] Smith D.R. *et al* 2008 *Rev. Sci. Instrum.* **79** 123501
[22] Mazzucato E. 2003 *Phys. Plasmas* **10** 753
[23] Mazzucato E. 2006 *Plasma Phys. Control. Fusion* **48** 1749
[24] Lao L.L. *et al* 1985 *Nucl. Fusion* **25** 1611
[25] Hosea J. *et al* 2008 *Phys. Plasmas* **15** 056104
[26] Coppi B. 2007 *Collective Phenomena in Macroscopic Systems* ed G. Bertin (Singapore: World Scientific)
[27] Yuh H.Y. *et al* 2009 private communication
[28] Mazzucato E. *et al* 1996 *Phys. Rev. Lett.* **77** 3145
[29] Kotschenreuther M., Rewoldt G. and Tang W.M. 1995 *Comput. Phys. Commun.* **88** 128
[30] Jenko F., Dorland W. and Hammett G.W. 2001 *Phys. Plasmas* **8** 4096
[31] Wang W.X. *et al* 2006 *Phys. Plasmas* **13** 092505